Hindawi
Shock and Vibration
Volume 2021, Article ID 5588056, 11 pages
https://doi.org/10.1155/2021/5588056

Research Article

Study on Flow Mechanism of a Morphing Supercritical Airfoil

Yuanjing Wang, Binbin Lv, Pengxuan Lei, Wenkui Shi, and Yu Yan

High Speed Aerodynamics Institute, China Aerodynamics Research and Development Center, Mianyang 621000, China

Correspondence should be addressed to Binbin Lv; lbin@cardc.cc

Received 7 January 2021; Revised 18 March 2021; Accepted 8 April 2021; Published 20 April 2021

Academic Editor: Zeqi Lu

In order to maintain the best performance in flight, a new concept, morphing aircraft, has been proposed, which can change the real-time aerodynamic characteristics under different flight conditions. The key problem is to figure out the response of strong flow instability caused by structure changes during the morphing. To solve this problem, computational fluid dynamics (CFD) and wind tunnel tests (WTT) were employed. The results show that the deformation of thickness and camber angle of the airfoil will significantly change the distribution of pressure and result in obvious hysteresis loops of lift and drag. With the increase of deformation frequency and amplitude, the instability increases correspondingly. Moreover, the unsteady effect caused by camber deformation is much stronger than that caused by thickness deformation. In addition, the flow structures on the airfoil, such as the shock strength and boundary separation location, have a delay in response to structure changes. Therefore, there will be a hysteresis between airfoil deformation and aerodynamic characteristics, which means strong flow instability.

1. Introduction

With the development of technology and science, more and more attentions have been paid to the quality and performance of aircrafts [1–3]. Nowadays, it is expected that changes in flow conditions have been adopted for aircraft configuration in order to maintain the optimal performance throughout the flight. Therefore, morphing airfoil is developed gradually. However, the impact of configuration changes on the flow structure and aircraft performance is not yet understood, which may hinder the progress of the morphing airfoil. Therefore, it is necessary to study the relationship and response law between the flow and configuration deformation.

Research institutes, such as NASA and DAPPA, have conducted long-term research on the related technologies of morphing vehicles [4–6], as well as a lot of research on aerodynamics. In the research of Ajaj et al. [7], the deformation technology was classified to put forward the concept of continuous deformation. Nekoubin and Nobari [8] calculated the deformation of the trailing edge of NACA0012 airfoil under the transonic condition and explained the influence of control parameters. Walker and Patil [9] derived the functions of unsteady lift, drag, and pitch moment and expressed them using the form of Chebyshev polynomials. Gandhi and Anusonti-Inthra [10] investigated the skin structure of variable camber wings. In the study of Adesen et al. [11], a dynamic stall model of variable trailing edge airfoil was derived based on the theory. As for domestic research, the development of morphing technology is later than foreign research. Xu et al. [12] proposed different types of morphing schemes for airfoils. Lv et al. [13, 14] conducted wind tunnel tests to study the aerodynamic characteristics under transonic conditions. Hao and Yang [15] analyzed the influence of camber change on steady-state and unsteady-state aerodynamic characteristics under low Reynolds number. Chen et al. [16] discussed the influence of wing sweep changes on aerodynamic features, as well as its mechanism. At the same time, using analytical and discrete vortex methods proposed by Gao et al. [17, 18], the unsteady aerodynamic characteristics of the morphing airfoil under subsonic/supersonic speed conditions were specifically studied.

The research on morphing technology mainly focuses on the design of intelligence structure [19, 20], but there are few studies on aerodynamic characteristics and flow mechanism

of morphing airfoil. Therefore, through CFD and wind tunnel tests, the influence of supercritical airfoil deformation on aerodynamic characteristics and flow structure has been discussed, and the results will be helpful for smart structure parameter choice and analysis on aerodynamic characteristics morphing airfoils.

2. Research Methods

2.1. Research Topic Introduction

2.1.1. The Issue and the Object. Typical supercritical airfoil designated by RAE2822 was chosen as the research target. Configuration of RAE2822 and its aerodynamic characteristics were plenty and open to researchers.

In this paper, effect of airfoil thickness and camber on its unsteady aerodynamic characteristics was studied by CFD simulation. When CFD was applied, the chord of RAE2822 was designated to 1 unit, based on which the parameters of the flow were obtained, such as the Reynolds number, and unsteady aerodynamic characteristics coefficients.

Only effect of airfoil camber changing through trailing edge deflection driven by a SMA smart structure on surface pressure distribution was measured in wind tunnel. Strictly speaking, this kind of deflection of wind tunnel model was not a real camber due to the difficulty in smart structure designing and wind tunnel experiments simulation. Experiment results could not be compared with those obtained by CFD, which was still helpful to recognize the flow phenomenon during model deformation in the wind tunnel environment. The model was extracted to a 2D wing based on RAE2822 airfoil, wing span and chord length of which were 365 mm and 150 mm, respectively (Figure 1).

2.1.2. Parameters for CFD Simulations. Aerodynamic characteristics of wing were decided by its airfoil parameters, of which airfoil camber and thickness were the most important parameters. Unsteady effect of morphing on aerodynamic characteristics over supercritical airfoil was mainly studied by CFD.

Flow structure and aerodynamic forces under different airfoil camber and thickness were simulated with Mach number ranging from 0.7 to 0.78, Reynolds number ranging from 5×10^6 to 30×10^6, and angles of attack ranging from 0° to 8°.

The variation of real-time airfoil thickness ranged from -15 percent to 20 percent of the basis airfoil thickness, and the angle which was used to measure airfoil camber between the chord trailing edge tangent and the horizontal axis ranged from -5° to 5°. Definition of airfoil thickness and camber would be introduced in Section 2.1.3. Camber and thickness morphing frequency ranged from 0 Hz to 2 Hz when the effect was simulated with CFD.

2.1.3. Contents in Wind Tunnel Experiments. When experiments were conducted in the wind tunnel, Mach number ranged from 0.4 to 0.8, test Reynolds number was kept at 2×10^6 approximately, and angles of attack ranged from 0° to 6°.

SMA material phase transition would result in the problem of slow response of smart structure, which made flow over supercritical airfoil kept in steady state during the trailing edge deflection. Wind tunnel experiments would be used only to recognize the steady flow structure evolution when trailing edge was deflected. Because of the effect of aerodynamic loads brought about by the dynamic pressure of the wind tunnel flow, the trailing edge deflection magnitude could not exceed 10.9°. It is not reasonable to compare wind tunnel experiment results with those obtained by CFD due to the different morphing mode and flow mode.

2.2. Computational Fluid Dynamic Method

2.2.1. CFD Methods. N-S equation based on finite volume was applied:

$$\iiint_{\Omega} \frac{\partial W}{\partial t} \, dV + \oiint_{\partial\Omega} H \cdot \vec{n} \, dS = 0. \tag{1}$$

The convective item was discretized with central scheme and the viscous item was discretized with ROE scheme. The time discretization of the unsteady-state calculation is carried out on the basis of the dual time step. When the maximum error of the basis variable quantity was less than 0.00001, the iteration was considered to be converged. At the same time, endless loop was avoided by designating inner time step. In addition, ideal-gas far field conditions were used as boundary conditions. The wall was adiabatic and nonslip. S-A turbulence model was applied.

2.2.2. Grid and Validation. C grid containing 941×144 grid nodes is used (Figure 2). In order to avoid the negative volume caused by chaotic deformation of large aspect ratio, the mesh field is divided into two parts, and only grid deformation is allowed. Since Reynolds number effect is not our main purpose, only characteristics are considered under full turbulence. $y+$ and the height of the first layer grid are 2 and 0.00002664, respectively.

The effectiveness of the steady method is verified according to Case 9 in the research of Zhang and Zhang [21], and the parameters are shown in Table 1. The comparison between the results of Case 9 and present study is shown in Table 2. The results are consistent with Case 9, showing that the steady method applied for the study was effective.

The effectiveness of the unsteady method is verified according to AGARD CT1 case [21], and the parameters are shown in Table 3.

The comparison of unsteady method with CT1 case is shown in Figure 3. It can be seen that dual time step discretization was qualified for unsteady computation; and the consistency of both results was well.

2.2.3. Timestep Determination. Lift coefficient under different timestep is shown in Figure 4. As can be seen, results of C_L coefficient were converged when real-time step size

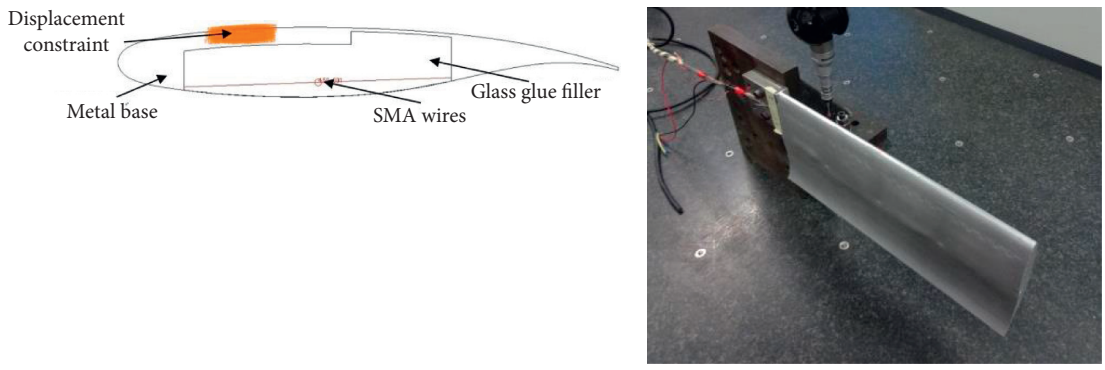

Figure 1: Sketch of the model.

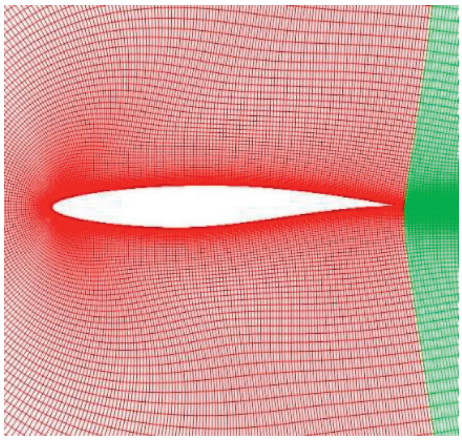

Figure 2: Grid of calculation field.

Table 1: Steady computational condition.

Flow condition	Mach number	Angles of attack (°)	Reynolds number
Case 9	0.734	2.79	1.0656×10^7

Table 2: Steady results of Case 9 and the present study.

	CL	Cd
EXP_Case 9	0.803	0.0168
Present study	0.804	0.0197

was larger than 1000. Therefore, inner iteration step size and the real time step size were assigned as 50 and 1000, respectively.

2.2.4. Definition of Airfoil Thickness and Camber Changes in CFD Simulation. The change of airfoil thickness is obtained by increasing the coordinates of all the original airfoil control points on average. Then, the coordinate equation of the control points is recommended:

$$Y = Y_{\text{init}} \times [1 + A \cdot \sin(2\pi f t)], \quad (2)$$

where Y_{init} is the initial coordinate of the airfoil control point, f is the deformation frequency of the airfoil thickness, and A is the relative amplitude of the thickness change, as shown in Figure 5.

It is difficult to express airfoil centerline equation algebraically. So, the airfoil chord was defined as a parabola to describe the camber. In order to keep the thickness constant during the camber change, the equation of camber changes is given as follows:

$$\begin{aligned} P &= A \cdot \sin(2\pi f t), \\ \Delta y &= -4Px^2 + 4Px, \end{aligned} \quad (3)$$

where P is the vertex instantaneous coordinate and Δy is the increase of the longitudinal coordinates of the surface control points. For convenience, the angle (θ) between the tangent of deformed chord at the trailing vertex and abscissa was used to measure chord camber changing. The camber change is shown in Figure 6.

2.3. Wind Tunnel Test

2.3.1. Facility. The test was conducted in a transonic wind with a Mach number ranging from 0.4 to 3.5. It is a semireturn wind transient wind tunnel with a cross-sectional dimension of 0.6×0.6 m. The upper and lower walls of this section are slotted, and the side walls are solid with rectangular optical windows and suitable for camera shooting.

2.3.2. Smart Actuator Structures. To understand the flow mechanism on morphing airfoils, a typical 2D supercritical airfoil test model was designed. The cantilever flexible flexure structure was applied to drive the trailing edge flexure. The structure is driven by a shape memory alloy (SMA) actuator, which can deflect the trailing edge by 10.9°. The cavity on the lower surface of the model was filled with glass glue to maintain the smoothness of the lower surface. In Figure 7, the SMA actuator model is recommended.

2.3.3. Test Technology. Since the lower surface was filled with glass glue, it is difficult to fix the pressure orifice. Therefore,

Table 3: Unsteady computational condition.

Flow condition	Mach number	Angles of attack (°)	Frequency reduction
CT1	0.6	2.89 + 2.41sin(w∗t)	0.0808

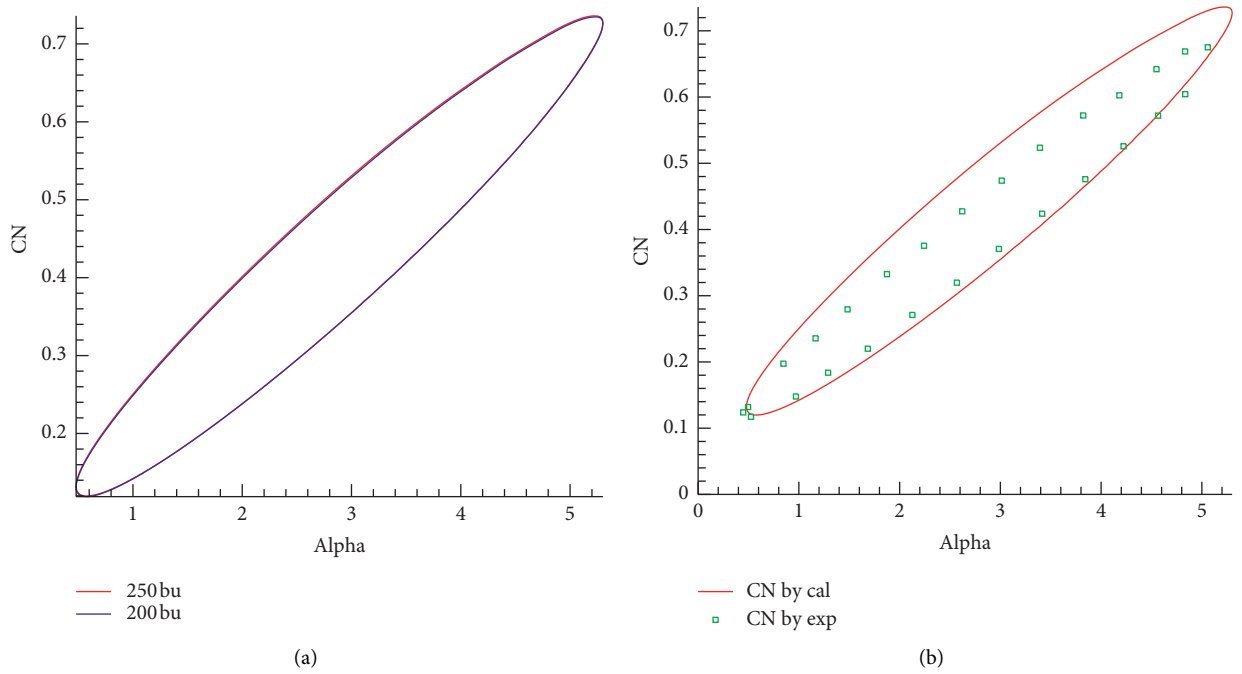

Figure 3: Numerical method and result compared with CT1 case.

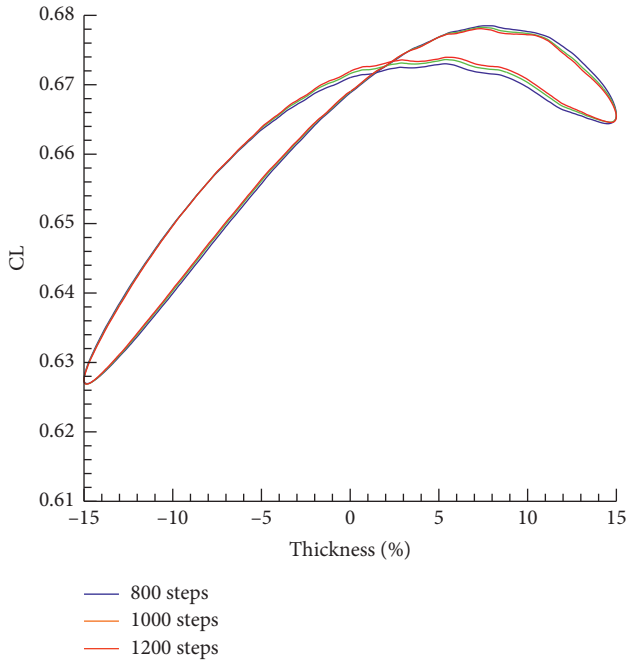

Figure 4: Comparison of C_L in different time step sizes ($M = 0.74$, $\alpha = 2^\circ$, and $F = 1$ Hz).

PSP technology was used to obtain the model surface pressure distribution under the condition of boundary layer natural transition. Image acquisition was composed of light source, camera, and control software. The excitation light source was a kind of LED cold light source with 12 W output power. The camera type was PCO.1600. In order to fix the deflection angle of the trailing edge, deformation measurement technology (VMD) was applied. In Figure 8, the position of the model in the test section is presented.

3. Results and Analysis

3.1. Influence of Thickness Deformation on Aerodynamic Characteristics. Figure 9 shows the influence of three thickness amplitudes (10%, 15%, and 20%) on the aerodynamic characteristics. It suggests that, with the increase of the deformation amplitude, the hysteresis phenomenon becomes more obvious, which is caused by the pressure and vorticity difference at the same position during the thickness deformation process (Figure 10). The area of the hysteresis loop formed by the lift coefficient can be understood as the work required by the external force during the deformation of airfoil. The greater the area, the greater the power required [22].

The influence of thickness deformation frequency is shown in Figure 11. The higher the deformation frequency, the greater the lift/drag force generated by the rate of change of the velocity potential over time. Within a certain range of frequency and amplitude, the difference between lift and drag is close to 0.015 and 0.0019, respectively, when the trailing edge passes through the same position of reciprocating motion.

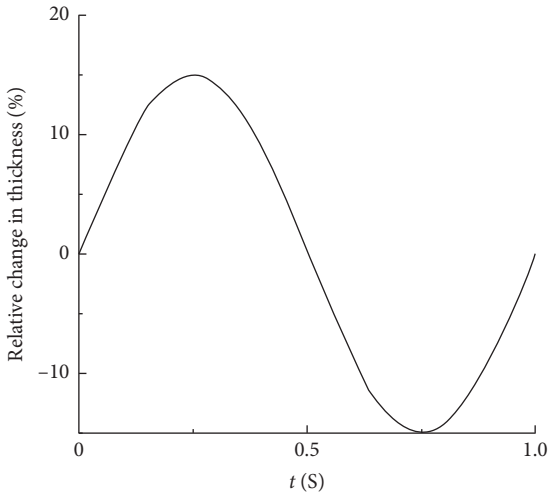

Figure 5: Relative change in thickness over time.

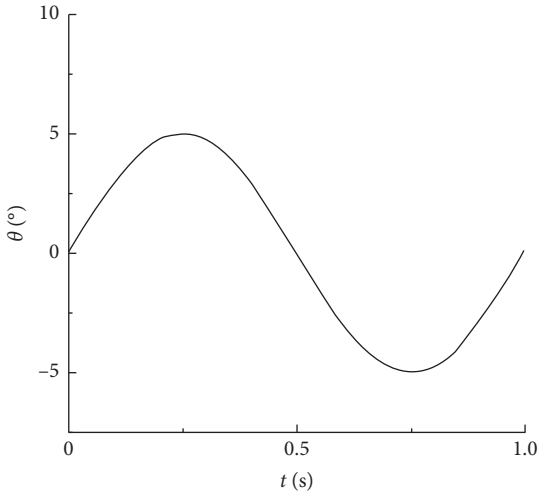

Figure 6: Camber changes over time.

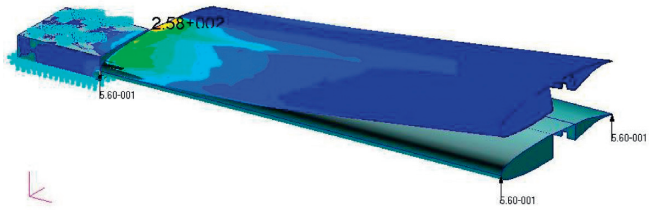

(a)

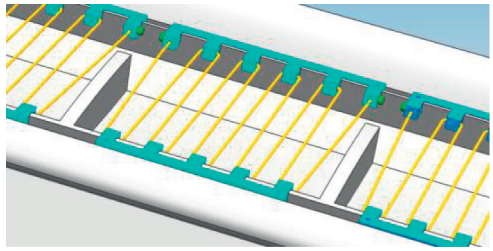

(b)

Figure 7: SMA actuator structure.

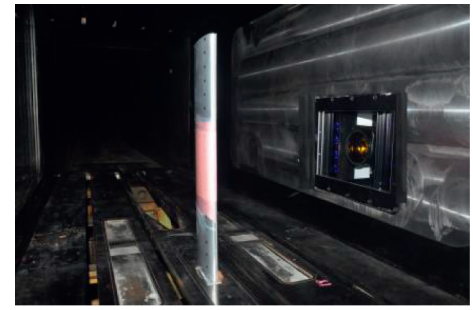

Figure 8: Model position in the test section.

3.2. Influence of Camber Deformation on Aerodynamic Characteristics. Figure 12 shows the influence of the extent of camber deformation on aerodynamics. It indicates that the larger the deformation, the stronger the unsteady-state effect and the larger the area of the hysteresis loop.

Figure 13 indicates that the higher the deformation frequency, the larger the area of the hysteresis loop, and the additional unsteady lift caused by the ratio of the velocity potential over time will also be greater.

When the angle of attack was increased to 6°, the same effect would be found as $\alpha = 2^{\circ}$. But, as can be seen in Figure 14, camber deformation would have less effect on aerodynamic characteristics at $\alpha = 6^{\circ}$ than at $\alpha = 2^{\circ}$; and the hysteresis characteristics of lift/drag force curves were not as regular at $\alpha = 6^{\circ}$ as at $\alpha = 2^{\circ}$. This resulted from the obvious shock wave and its induced boundary layer separation. As can be seen in Figure 15, strong separation happened, and position of flow separation moved forward when camber changing magnification angle θ was -3° again. We could obtain that flow structures were very different at the same position but different time. That was the unsteady flow that led to the hysteresis characteristics of lift/drag forces during morphing.

The above results show that the airfoil thickness and camber deformation will cause obvious instability, and the aerodynamic coefficient has obvious hysteresis characteristics. Moreover, the greater the amplitude of the airfoil parameter deformation and the higher the frequency, the stronger the flow instability. By comparing it with thickness deformation, the change of the camber angle will cause more severe instability, which will lead to greater additional instability. For example, the difference between lift and drag is close to 0.117 and 0.0034, respectively, which indicates that the instability of vehicle deformation should not be ignored.

3.3. Mechanism of Unsteady Flow during Airfoil Deformation. The effect of deformation on the surface pressure distribution is shown in Figure 12, which indicates that when the trailing edge returns to pass through the same position, the shock wave moves to the airfoil nose and its strength is weakened. This is caused by the hysteresis and strength of the shock wave position relative to geometric deformation. This phenomenon can also be observed in the PSP wind tunnel test results (Figure 16). It can be seen that, with the deflection of the trailing edge, the shock wave has been strengthened and pushed back. The flow near the center of

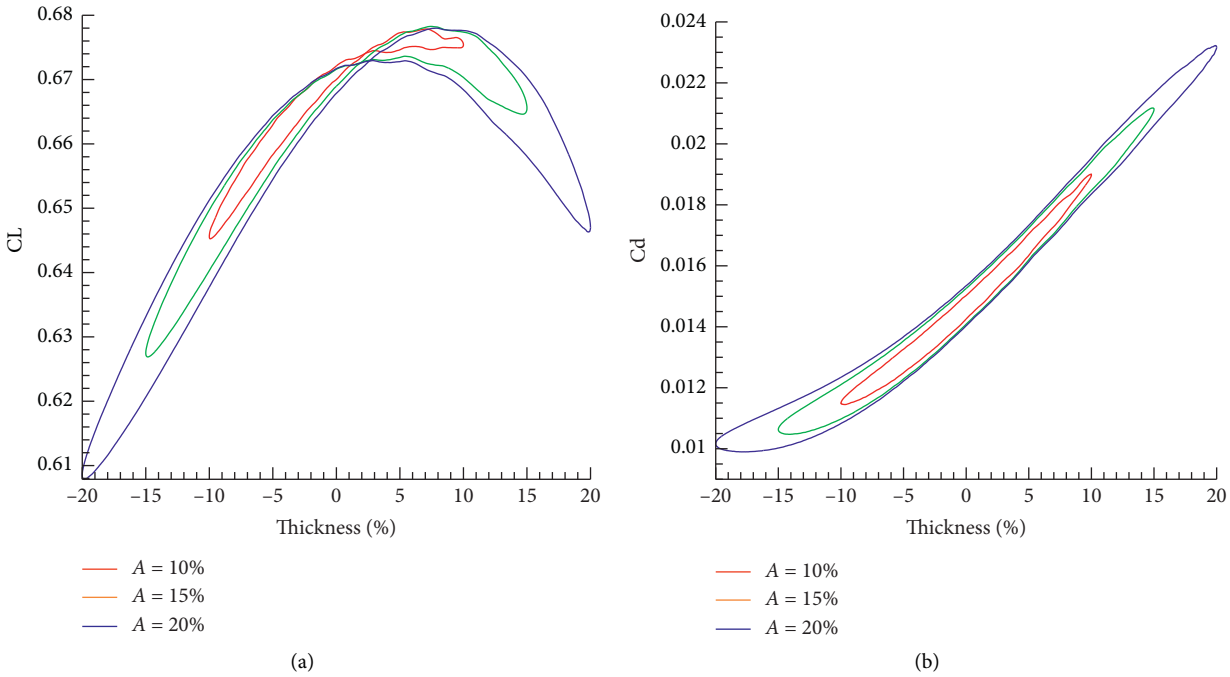

Figure 9: Influence of thickness deformation amplitude on aerodynamics ($M = 0.74$, $\alpha = 2^{\circ}$, and $f = 1$ HZ, CFD).

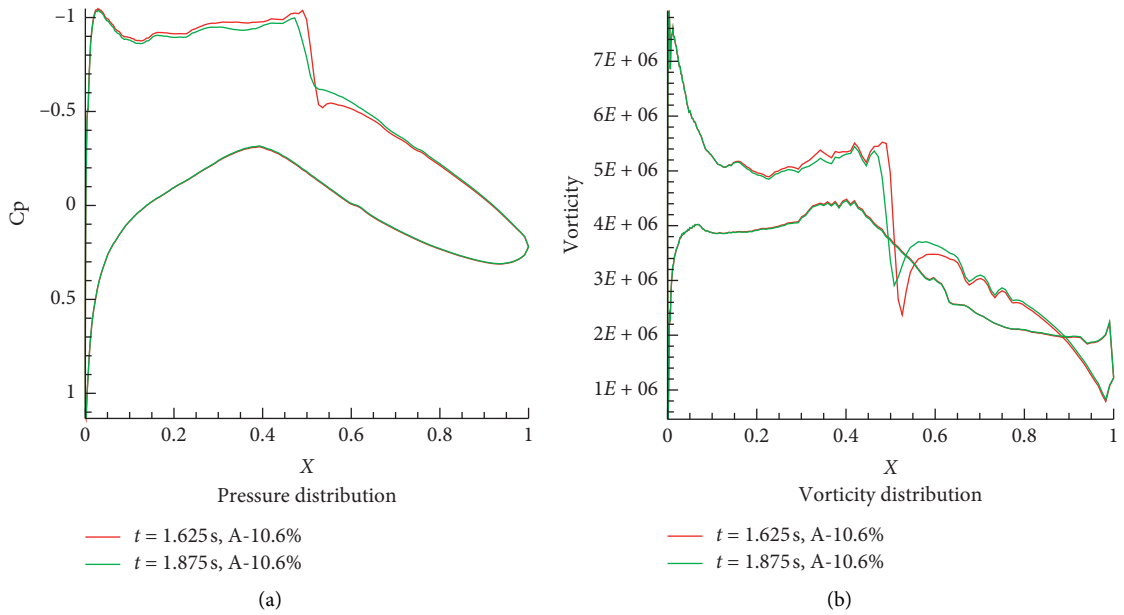

Figure 10: Pressure and vortex distribution at the same thickness (−10.6%) in one cycle ($M = 0.74$ and $\alpha = 2^{\circ}$, CFD). (a) Pressure distribution. (b) Vorticity distribution.

rotation accelerates again and shows a tendency to form a second shock wave.

The influence of deformation on the surface pressure distribution is shown in Figure 12, which indicates that when the trailing edge returns to pass through the same position, the shock wave moves to the airfoil nose and its strength is weakened. This is caused by the hysteresis and strength of the shock wave position relative to geometry deformation. This phenomenon can also be observed from PSP wind tunnel test results (Figure 17). It can be seen that, with the deflection of the trailing edge, the shock wave has been strengthened and pushed back. The flow near the center of rotation center accelerates again and shows a tendency to form the second shock wave.

Figure 18 shows how the amplitude and frequency of airfoil camber deformation affect the surface pressure distribution. The graph shows that larger amplitude and higher frequency will cause larger changes in pressure distribution.

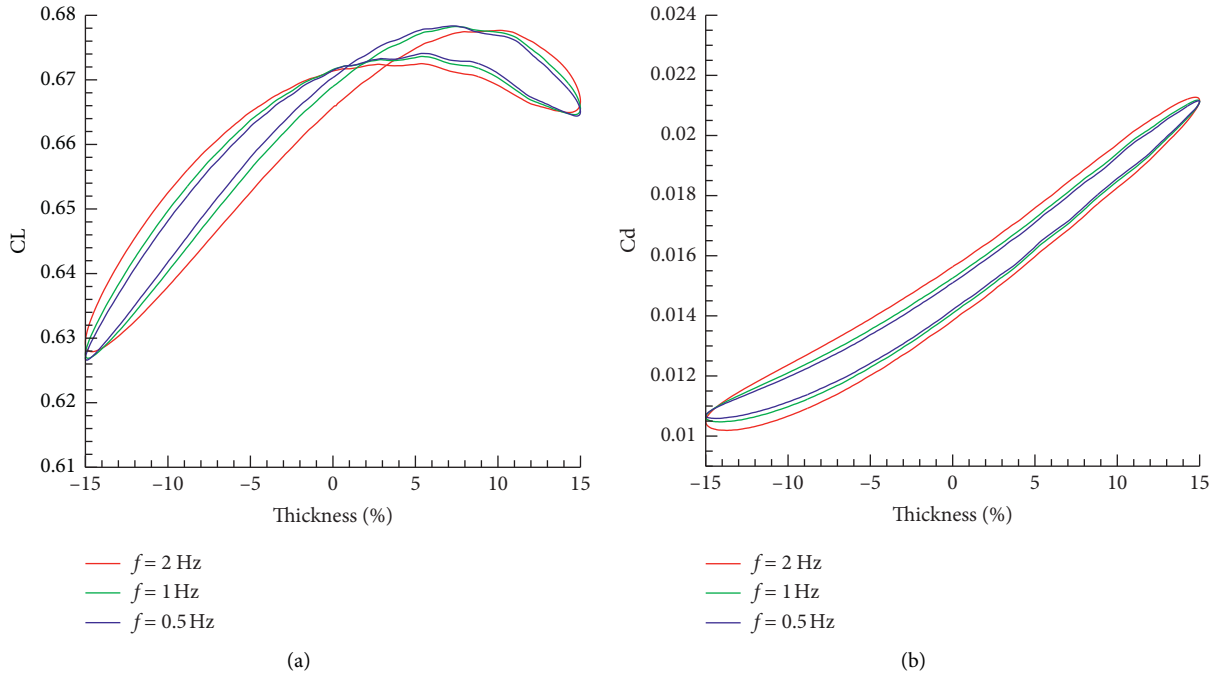

Figure 11: Influence of thickness deformation frequency on aerodynamics ($M = 0.74$ and $\alpha = 2^{\circ}$, CFD).

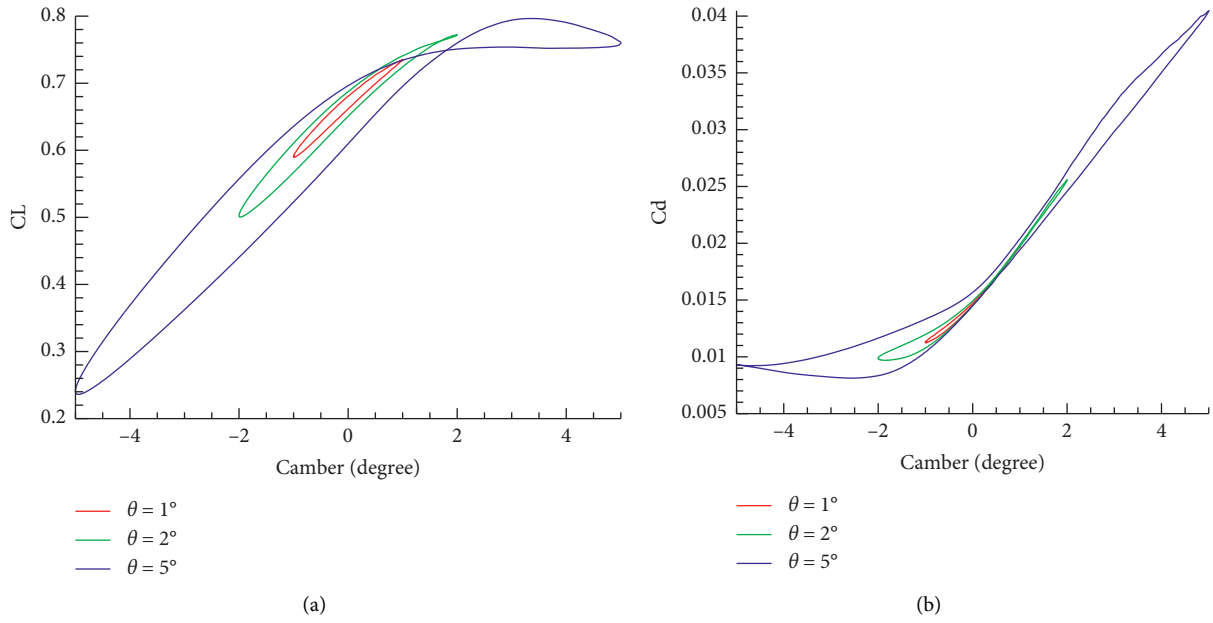

Figure 12: Influence of the extent of camber deformation on aerodynamics ($M = 0.74$, $\alpha = 2^{\circ}$, and $f = 1$ HZ, CFD).

For instance, such change can significantly enhance the shock wave and move the shock wave to the end of the airfoil, resulting in the increased unstable additional lift.

The results show that the unsteady flow effect in the wing morphing process is caused by flow separation, boundary layer transition, shock wave oscillation, and so forth. In the research of Yang [23], the author believes that the aerodynamics of an unsteady morphing airfoil can be represented by a constant item and a stable item. The additional unstable item is shown as

$$F_x - iF_y = -i\oint_{l_b} \rho\left[c\mathrm{d}\overline{z} - \frac{\partial \overline{x}}{\partial t}\mathrm{d}\overline{z} - \frac{1}{2}\cdot\left(\frac{\partial x}{\partial z}\right)^2 \mathrm{d}z\right]. \quad (4)$$

In the process of airfoil deformation, the rate of velocity potential change will cause virtual mass force, which may lead to unstable additional force. Because the velocity change rate of the airfoil parameters is different, the unstable additional force/moment is also different, thus forming a hysteresis loop.

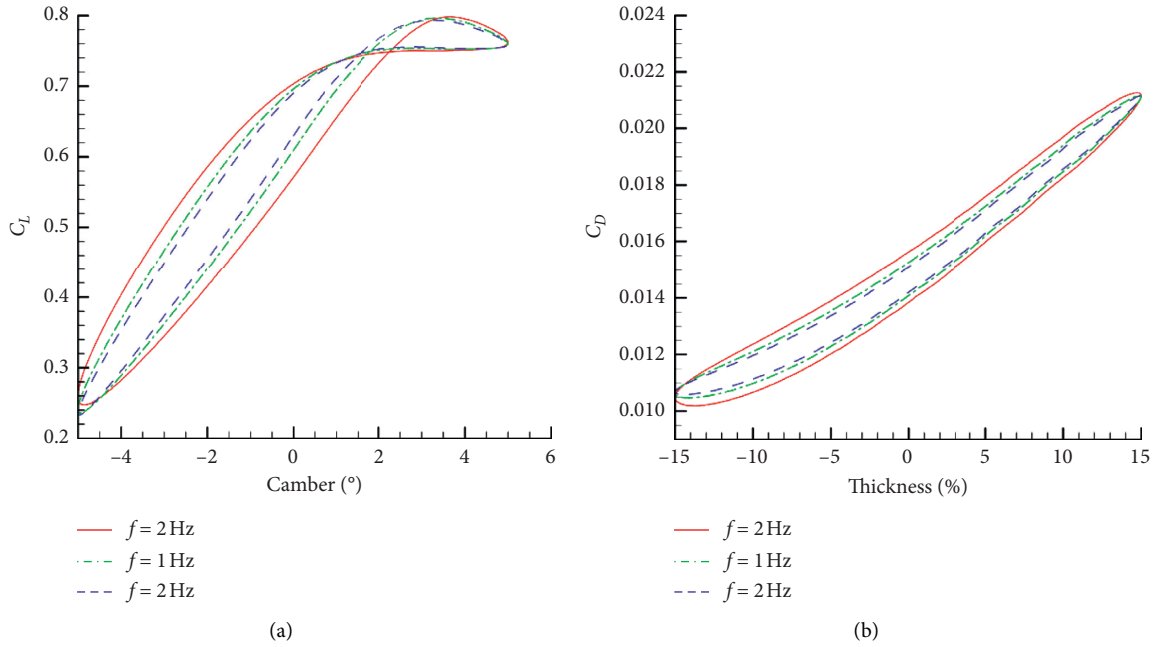

FIGURE 13: Influence of camber deformation frequency on aerodynamics ($M = 0.74$ and $\alpha = 2^{\circ}$, CFD).

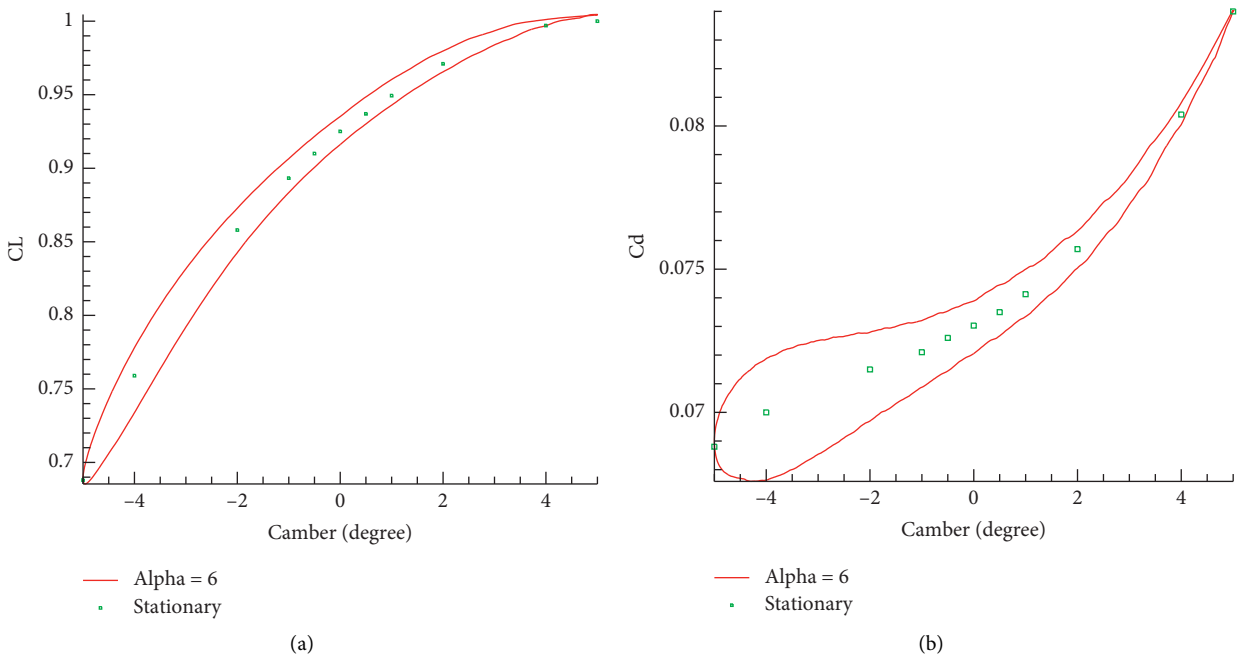

FIGURE 14: Influence of camber changing on aerodynamics ($M = 0.74$, $\alpha = 6^{\circ}$, and $f = 1$ Hz, CFD).

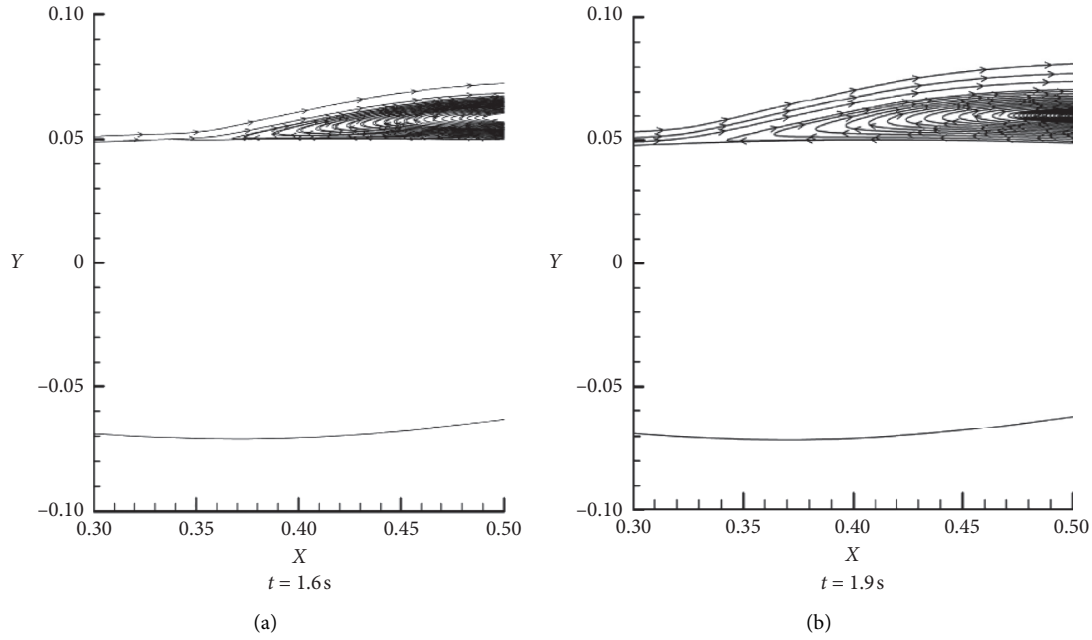

Figure 15: Streamline over leeward flow field of the airfoil at the same camber (−3°) in one cycle ($M = 0.74$, $\alpha = 6°$, and $f = 1$ Hz, CFD).

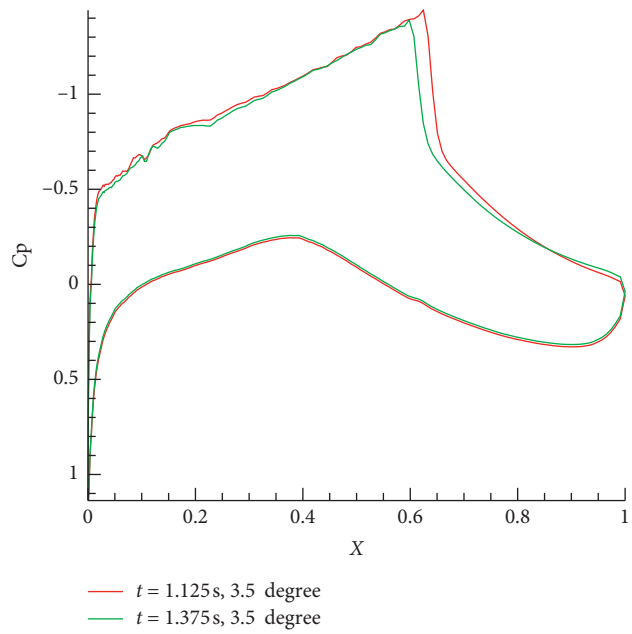

Figure 16: Pressure distribution passing through the same camber position in one cycle ($M = 0.74$, $\alpha = 2°$, and $\theta = 3.5°$, CFD).

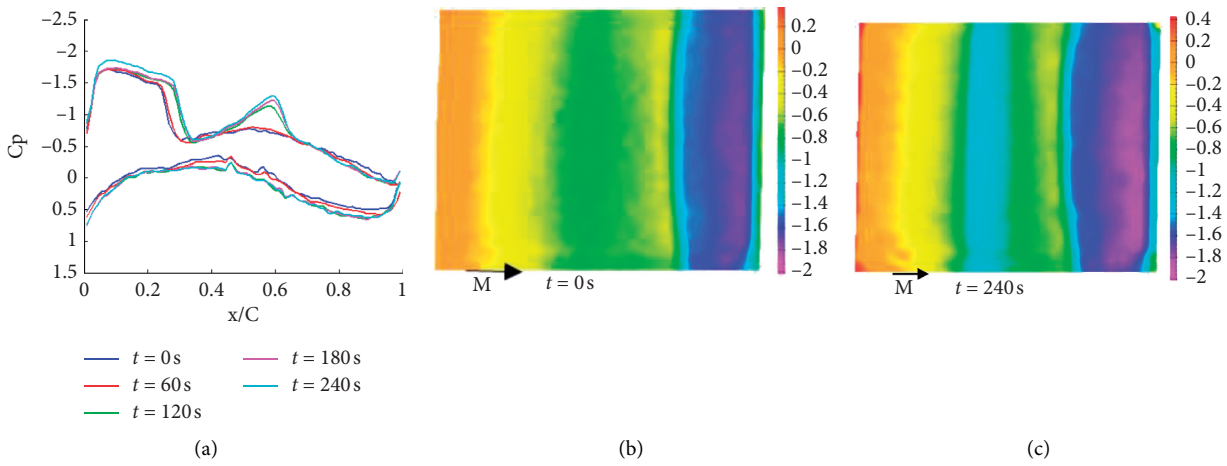

Figure 17: Wind tunnel test results (PSP, $M = 0.7$ and $\alpha = 6^{\circ}$, test).

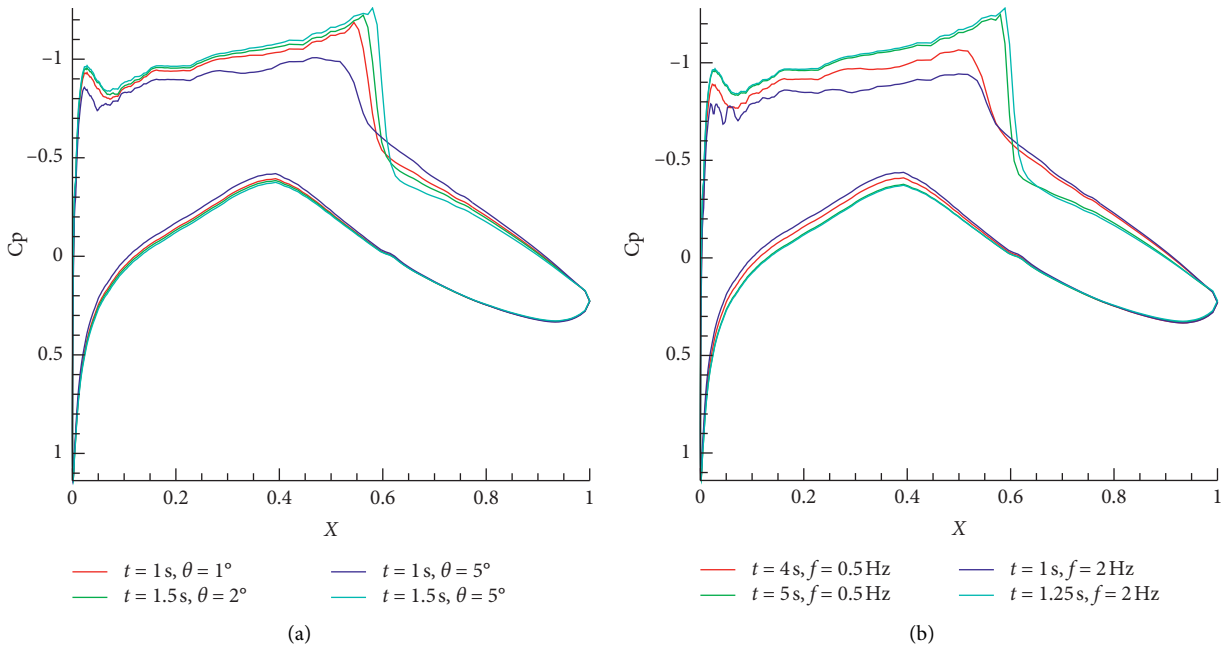

Figure 18: Influence of camber deformation on pressure distribution (CFD).

4. Conclusions

In this study, the influence of the thickness and camber deformation of the supercritical airfoil on flow instability and its mechanism was studied. The conclusions can be drawn as follows:

(1) Flow instability will occur with the change of airfoil thickness and camber angle, and it exhibits obvious hysteresis on the aerodynamics forces of the hysteresis loop. Therefore, in the design of morphing aircrafts, full attention must be paid to the unsteady aerodynamic characteristics of deformation.

(2) Larger morphing amplitude and higher morphing frequency will lead to stronger flow hysteresis and unstable effects. Compared with the influence of airfoil thickness deformation, the instability caused by airfoil camber deformation is more significant, which cannot be ignored.

(3) The flow instability originates from the response of the position and intensity of shock wave and the boundary separation characteristics to geometric deformation. It may result in obvious additional aerodynamic forces.

Data Availability

The data were measured in the wind tunnels at High Speed Aerodynamics Institute, China Aerodynamics Research and Development Center.

Conflicts of Interest

The authors declare that they have no conflicts of interest.

References

[1] M. Secanell, A. Suleman, and P. Gamboa, "Design of a morphing airfoil for a light unmanned aerial vehicle using high-fidelity aerodynamics shape optimization," in *Proceedings of the 46th AIAA/ASME/ASCE/AHS/ASC Structures, Structural Dynamics and Materials Conference*, Austin, TX, USA, April 2005.

[2] E. J. Cui, B. Peng, and J. M. Yang, "Development road of smart morphing aircraft," *Aeronautical Manufacturing Technology*, vol. 8, pp. 38–41, 2007.

[3] Z.-Q. Lu, K.-K. Zhang, H. Ding, and L.-Q. Chen, "Internal resonance and stress distribution of pipes conveying fluid in supercritical regime," *International Journal of Mechanical Sciences*, vol. 186, Article ID 105900, 2020.

[4] J. Florance, G. Fleming, A. Burner et al., "Contributions of the NASA langley research center to the DARPA/AFRL/NASA/ northrop grumman smart wing program," in *Proceedings of the 44th AIAA/ASME/ASCE/AHS/ASC Structures, Structural Dynamics, and Materials Conference*, Norfolk, VA, USA, April 2003.

[5] Z.-Q. Lu, D.-H. Gu, H. Ding, W. Lacarbonara, and L.-Q. Chen, "Nonlinear vibration isolation via a circular ring," *Mechanical Systems and Signal Processing*, vol. 136, Article ID 106490, 2020.

[6] J. N. Kudva, "Overview of the DARPA smart wing project," *Journal of Intelligent Material Systems and Structures*, vol. 15, no. 4, pp. 261–267, 2004.

[7] R. M. Ajaj, C. S. Beaverstock, and M. I. Friswell, "Morphing aircraft: the need for a new design philosophy," *Aerospace Science and Technology*, vol. 49, pp. 154–166, 2016.

[8] N. Nekoubin and M. R. H. Nobari, "Numerical investigation of transonic flow over deformable airfoil with plunging motion," *Applied Mathematics and Mechanics*, vol. 37, no. 1, pp. 75–96, 2016.

[9] W. P. Walker and M. J. Patil, "Unsteady aerodynamics of deformable thin airfoils," *Journal of Aircraft*, vol. 51, no. 6, pp. 1673–1680, 2014.

[10] F. Gandhi and P. Anusonti-Inthra, "Skin design studies for variable camber morphing airfoils," *Smart Materials and Structures*, vol. 17, no. 1, Article ID 015025, 2008.

[11] P. B. Andersen, M. Gaunaa, C. Bak et al., "A dynamic stall model for airfoils with deformable trailing edges," *Journal of Physics: Conference Series*, vol. 75, no. 1, Article ID 012028, 2007.

[12] G. W. Xu, B. Peng, and S. Wen, "Primary research of morphing scheme over 2D airfoil," *Chinese Quarterly of Mechanics*, vol. 4, pp. 570–576, 2011.

[13] B. B. Lv, P. X. Lei, Y. J. Wang et al., "Research on the aerodynamic characteristics of morphing super-critical airfoil airfoil," *Asia-Pacific International Symposium on Aerospace Technology*, pp. 828–835, Springer, Singapore, 2018.

[14] W. K. Shi, Y. J. Wang, and Z. Zhang, "Unsteady aerodynamic characteristics of deformable supercritical airfoil," *Acta Aerodynamic Sinica*, vol. 35, no. 2, pp. 192–197, 2017.

[15] N. S. Hao and W. C. Yang, "Experimental study of unsteady aerodynamic characteristics of variable camber wing at low reynolds number," *Journal of Experimental Mechanics*, vol. 3, pp. 294–301, 2014.

[16] Q. Chen, B. Peng, and L. Feng, "Morphing aircraft wing variable sweep: two practical methods and their aerodynamic characteristics," *Acta Aero-Dynamical Sinia*, vol. 30, no. 5, pp. 658–663, 2012.

[17] Y. F. Gao, Z. Liu, and X. Wang, "Study on the supersonic unsteady aerodynamic force for the morphing airfoil," *Acta Aero-Dynamical Sinia*, vol. 685, pp. 69–76, 2014.

[18] Y. F. Gao, X. Wang, and Z. Liu, "Study on the subsonic unsteady aerodynamic force for the morphing Joukowski airfoil," *Chinese Quarterly of Mechanics*, vol. 11, pp. 1–9, 2012.

[19] Z.-Q. Lu, D. Wu, H. Ding, and L.-Q. Chen, "Vibration isolation and energy harvesting integrated in a Stewart platform with high static and low dynamic stiffness," *Applied Mathematical Modelling*, vol. 89, pp. 249–267, 2021.

[20] Z.-Q. Lu, K.-K. Zhang, H. Ding, and L.-Q. Chen, "Nonlinear vibration effects on the fatigue life of fluid-conveying pipes composed of axially functionally graded materials," *Nonlinear Dynamics*, vol. 100, no. 2, pp. 1091–1104, 2020.

[21] Y. F. Zhang and X. L. Zhang, "Credibility analysis of RAE 2822 airfoil transonic flow computation," *Aeronautical Computing Technique*, vol. 39, no. 4, pp. 68–70, 2009.

[22] Y. F. Gao, *Study on the Unsteady Aerodynamics Characteristics for the Morphing Airfoil*, University of Science and Technology of China, Hefei, China, 2012.

[23] W. C. Yang, *Experimental Investigation on the Flow Separation Behaviours of a Variable Camber Wing*, University of Science and Technology of China, Hefei, China, 2012.